



Delft University of Technology

Evidence of regional sea-level rise acceleration for the North Sea

Steffelbauer, David B.; Riva, Riccardo E.M.; Timmermans, Jos S.; Kwakkel, Jan H.; Bakker, Mark

DOI

[10.1088/1748-9326/ac753a](https://doi.org/10.1088/1748-9326/ac753a)

Publication date

2022

Document Version

Final published version

Published in

Environmental Research Letters

Citation (APA)

Steffelbauer, D. B., Riva, R. E. M., Timmermans, J. S., Kwakkel, J. H., & Bakker, M. (2022). Evidence of regional sea-level rise acceleration for the North Sea. *Environmental Research Letters*, 17(7), Article 074002. <https://doi.org/10.1088/1748-9326/ac753a>

Important note

To cite this publication, please use the final published version (if applicable). Please check the document version above.

Copyright

Other than for strictly personal use, it is not permitted to download, forward or distribute the text or part of it, without the consent of the author(s) and/or copyright holder(s), unless the work is under an open content license such as Creative Commons.

Takedown policy

Please contact us and provide details if you believe this document breaches copyrights. We will remove access to the work immediately and investigate your claim.

LETTER • OPEN ACCESS

Evidence of regional sea-level rise acceleration for the North Sea

To cite this article: David B Steffebauer *et al* 2022 *Environ. Res. Lett.* **17** 074002

View the [article online](#) for updates and enhancements.

You may also like

- [Search for Gravitational Waves Associated with Gamma-Ray Bursts Detected by Fermi and Swift during the LIGO–Virgo Run O3b](#)
R. Abbott, T. D. Abbott, F. Acernese et al.
- [Narrowband Searches for Continuous and Long-duration Transient Gravitational Waves from Known Pulsars in the LIGO–Virgo Third Observing Run](#)
R. Abbott, T. D. Abbott, F. Acernese et al.
- [GaN-based quasi-vertical Schottky barrier diode hybridized with p-NiO layer to achieve 1.1 kV breakdown voltage and enhance the current spreading effect](#)
Fuping Huang, Chunshuang Chu, Zhizhong Wang et al.

ENVIRONMENTAL RESEARCH
LETTERS

LETTER

Evidence of regional sea-level rise acceleration for the North Sea

OPEN ACCESS

RECEIVED
19 January 2022REVISED
18 May 2022ACCEPTED FOR PUBLICATION
1 June 2022PUBLISHED
14 June 2022

Original Content from
this work may be used
under the terms of the
[Creative Commons
Attribution 4.0 licence](#).

Any further distribution
of this work must
maintain attribution to
the author(s) and the title
of the work, journal
citation and DOI.

David B Steffelbauer^{1,2} , Riccardo E M Riva^{3,*} , Jos S Timmermans⁴ , Jan H Kwakkel⁴ and Mark Bakker¹ ¹ Water Management Department, Faculty of Civil Engineering and Geosciences, Delft University of Technology, Stevinweg 1, 2628 CN Delft, The Netherlands² Kompetenzzentrum Wasser Berlin, Cicerostrasse 24, 10709 Berlin, Germany³ Department of Geoscience and Remote Sensing, Faculty of Civil Engineering and Geosciences, Delft University of Technology, Stevinweg 1, 2628 CN Delft, The Netherlands⁴ Multi-Actor Systems Department, Faculty of Technology, Policy and Management, Delft University of Technology, Jaffalaan 5, 2628 BX Delft, The Netherlands

* Author to whom any correspondence should be addressed.

E-mail: R.E.M.Riva@tudelft.nl**Keywords:** sea-level rise, breakpoint detection, regional acceleration, timely adaptationSupplementary material for this article is available [online](#)**Abstract**

Global mean sea-level rise (SLR) has accelerated since 1900 from less than 2 mm yr⁻¹ during most of the century to more than 3 mm yr⁻¹ since 1993. Decision-makers in coastal countries, however, require information on SLR at the regional scale, where detection of an acceleration in SLR is difficult, because the long-term sea-level signal is obscured by large inter-annual variations with multi-year trends that are easily one order of magnitude larger than global mean values. Here, we developed a time series approach to determine whether regional SLR is accelerating based on tide gauge data. We applied the approach to eight 100-year records in the southern North Sea and detected, for the first time, a common breakpoint in the early 1990s. The mean SLR rate at the eight stations increases from 1.7 ± 0.3 mm yr⁻¹ before the breakpoint to 2.7 ± 0.4 mm yr⁻¹ after the breakpoint (95% confidence interval), which is unprecedented in the regional instrumental record. These findings are robust provided that the record starts before 1970 and ends after 2015. Our method may be applied to any coastal region with tidal records spanning at least 40 years, which means that vulnerable coastal communities still have time to accumulate the required time series as a basis for adaptation decisions in the second half of this century.

1. Introduction

Sea level rise (SLR) is threatening coastal communities worldwide. The ability of a society to adapt in a timely manner hinges on the timely detection of changes in key driving forces (Bloemen *et al* 2018, Richter *et al* 2020). Of particular relevance for coastal adaptation is the detection of an acceleration in regional SLR, which either requires a more rapid adaptation of coastal defense structures (Haasnoot *et al* 2020) or a shift in strategy from holding the line to managed coastal retreat (Haasnoot *et al* 2021, Mach and Siders 2021, Moss *et al* 2021). Both satellite altimetry observations and sea-level reconstructions based on tide gauge data show that global mean SLR has been accelerating through the 20th century (Dangendorf *et al* 2017, 2019, Frederikse *et al* 2020).

However, global mean SLR values are not salient for decision makers in coastal countries, who require SLR data at the regional scale (Cash *et al* 2003, Haasnoot *et al* 2018) to plan for timely adaptation.

The detection of acceleration in regional SLR is a major challenge, because sea-level measurements are affected by region-specific physical processes such as winds, shallow-ocean dynamics, river runoff, and bathymetry changes (Vinogradov and Ponte 2011, Frederikse *et al* 2016, Davis and Vinogradova 2017, Raso *et al* 2019a, 2019b). In the North Sea, detection of an acceleration in SLR is particularly challenging because the region is located within a shallow continental shelf, where a large inter-annual to decadal variability is induced by the combined effect of local atmospheric conditions and off-shelf ocean dynamics (Dangendorf *et al* 2014). Previous studies

of the North Sea region applied various time series approaches to analyze SLR (Calafat and Chambers 2013, Wahl *et al* 2013, Haigh *et al* 2014, Ezer *et al* 2016), but were not able to find evidence of a significant acceleration in the studied records.

In this paper, we developed a two-step approach to detect a potential acceleration in tidal records. First, we extract the sea-level signal from tide gauge data. And second, we analyze the extracted sea-level signal to detect whether a breakpoint is present, and to quantify the SLR before and after the breakpoint. We applied this approach to eight tide gauges in the North Sea, where several stations provide high-quality and uninterrupted records spanning more than a century. The robustness of the results was carefully evaluated by analyzing parts of the time series with different beginning and end years.

2. Methods

We developed a two-step approach to detect a possible acceleration in SLR from tide gauge data. The first step is to extract the sea-level signal (i.e. the signature of steric and barostatic SLR) from tide gauge data using an unobserved components model (UCM). The second step is to detect a possible acceleration by fitting a piecewise linear function (PWLf) to the extracted sea-level signal. The slope of each linear segment represent the rate of SLR. A breakpoint in the PWLf represents a change in SLR rate; an increase in the slope represents an acceleration.

2.1. Step 1: extraction of the sea-level signal

Periodical, external, and random influences obscure the sea-level signal in raw tide gauge data. We developed an UCM (Harvey 1990) to extract the sea-level signal from monthly averaged tide gauge data. The UCM models the tide gauge data y_t as a superposition of the sea-level signal μ_t , M seasonal variations $\gamma_{m,t}$, N external influencing factors $X_{n,t}$ with corresponding coefficients β_n , and a random component ϵ_t :

$$y_t = \mu_t + \sum_{m=1}^M \gamma_{m,t} + \sum_{n=1}^N \beta_n X_{n,t} + \epsilon_t. \quad (1)$$

The sea-level signal is modeled with a local level model (a random walk process)

$$\mu_{t+1} = \mu_t + \eta_t \quad (2)$$

where η_t are identically distributed random variables with zero mean and finite standard variance, which are mutually independent of ϵ_t and μ_t .

Two seasonal signals are taken into account ($M=2$): the lunar nodal cycle $\gamma_{1,t}$ and a yearly variation $\gamma_{2,t}$. The lunar nodal cycle is the main tidal component at decadal scale with a period of 18.61 years (Kaye and Stuckey 1973). The low-frequency nodal

tide is not accurately resolvable, since large-scale ocean dynamics and global land hydrology have multi-decadal cycles of comparable periods. Hence, we follow Woodworth (2012) and correct for its effect by removing the theoretical equilibrium tide upfront, before applying the UCM. The nodal tide is calculated as

$$\gamma_{1,t} = a \cos\left(\frac{2\pi}{\lambda_n} t - \phi_n\right) \quad (3)$$

where time t is in years, the equilibrium tide amplitude a is in mm, the nodal period λ_n is 18.61 years, and the nodal phase ϕ_n is the year 1922.7. The amplitudes are taken from Frederikse *et al* (2016) and depend on the latitude and the longitude of the tidal station. The yearly variation is modeled as a repeating pattern in the time domain ($\gamma_{2,t+s} = \gamma_{2,t}$) with periodicity $s=12$ months. The yearly variation sums up to zero over a complete cycle (Durbin and Koopman 2013)

$$\gamma_{2,t} = -\sum_{j=1}^{s-1} \gamma_{2,t-j}. \quad (4)$$

The effect of an external influence factor $X_{n,t}$ is simulated as $\beta_n X_{n,t}$ where β_n is a regression parameter. For our analysis, we model the effect of three external factors ($N=3$) for each individual station: the atmospheric pressure $X_{1,t} = p_t$, the wind stress $X_{2,t} = \tau_{u,t}$ in zonal u_t wind direction, and the wind stress $X_{3,t} = \tau_{v,t}$ in meridional v_t wind direction (Frederikse and Gerkema 2018)

$$\tau_{u,t} \propto u_t \cdot \sqrt{u_t^2 + v_t^2} \quad (5)$$

$$\tau_{v,t} \propto v_t \cdot \sqrt{u_t^2 + v_t^2}. \quad (6)$$

All three external factors are standardised by subtracting the mean and dividing by the standard deviation. Moreover, a variance inflation factor test (James *et al* 2013) showed no strong collinearities between the three external factors (table S1, supplemental material). Hence, the factors can be treated as being independent of each other.

Finally, the irregular component (error or disturbance) $\epsilon_t(t)$ is modeled as an independent and identically distributed random variable with zero mean and finite and constant variance σ_ϵ^2 (Durbin and Koopman 2013). The Python package ‘statsmodels’ was used to fit the UCM (Seabold and Perktold 2010). Regression coefficients are estimated by maximum likelihood via a Kalman filter. All external influencing factors and the seasonal components are significant according to their p -values and 95% confidence intervals.

2.2. Step 2: detection of an acceleration in the sea-level signal

Change-point and breakpoint functions are commonly used to detect non-linear behavior in climate data (Mudelsee 2019). We search for a possible acceleration in SLR by fitting a PWLF consisting of two segments to the extracted sea-level signal μ_t . A breakpoint in the PWLF represents a change (acceleration) in SLR. We fit a PWLF rather than a quadratic function, because climate-related time series might show abrupt rate changes, while a quadratic function represents a constant acceleration that is highly dependent on the length of the analyzed time series (Haigh *et al* 2014).

The PWLF is written as

$$\hat{\mu}_t = k_1 t + d \quad \text{for } t < t^* \quad (7)$$

$$\hat{\mu}_t = k_2 t + d - (k_2 - k_1)t^* \quad \text{for } t \geq t^* \quad (8)$$

where t^* is the breakpoint, k_1 is the slope before the breakpoint, k_2 is the slope after the breakpoint, and d is the intercept (time is standardised to zero at the first measurement). Note that the time derivative of the PWLF is discontinuous at the breakpoint t^* .

The posterior distribution of the regression parameters of the PWLF and their corresponding uncertainties are estimated using Bayesian inference. The coefficients of all N_s tidal stations, all with the same breakpoint t^* , are estimated simultaneously. The parameters k_1 , k_2 , and d may differ between stations because of local differences. All parameters are gathered in a vector θ . The difference between the data vector μ and the fit vector $\hat{\mu}(\theta)$ is approximated by a Gaussian distribution $\mathcal{N}(0, \sigma^2)$ where the standard deviation σ is the same for all stations because they all have similar variability. The parameter vector for N_s tide gauges has length $3N_s + 2$: k_1 , k_2 and d for each station, one common breakpoint t^* for all stations, and the standard deviation σ .

The parameters are estimated using the Markov Chain Monte Carlo method. Uniform priors are used for all parameters. The boundaries of the priors are chosen in such a way that they correspond to weak information regarding the true parameter values. k_1 may vary between 0 and $k_{\max} = 6 \text{ mm yr}^{-1}$, k_2 may vary between k_1 and k_{\max} , so that we restrict the algorithm to look only for accelerations and not decelerations in SLR. The intercept d may vary between plus and minus twice the maximum value of μ , which is a conservative boundary. The breakpoint t^* may vary between the starting time t_s and end time t_e of the time series, and σ may vary between 2 and 200 mm yr^{-1} .

The Metropolis-Hastings algorithm is used to sample t^* , which is not differentiable. The No-U-Turn Sampler (Hoffman and Gelman 2014), which is an algorithm that takes advantage of information about regions of higher probability based on the

gradient of the log posterior-density, is used to sample all other (continuous) variables; this helps to achieve significantly faster convergence (Salvatier *et al* 2016).

The developed Bayesian inference breakpoint detection algorithm is implemented in Python using the *PyMC3* package (Salvatier *et al* 2016). We used four parallel chains, each with 4000 steps for parameter tuning and subsequently 10 000 sampling steps. The step size is tuned to a target acceptance probability of 0.9. The tuning steps and the first 20% of the sampling steps are discarded from the final distribution, so that 32 000 samples are obtained to represent the posterior distribution for each parameter. Finally, a robustness check is performed to determine whether the detected breakpoint and SLR acceleration depends on the length of the time series.

2.3. Tide gauges and meteorological data for the North Sea

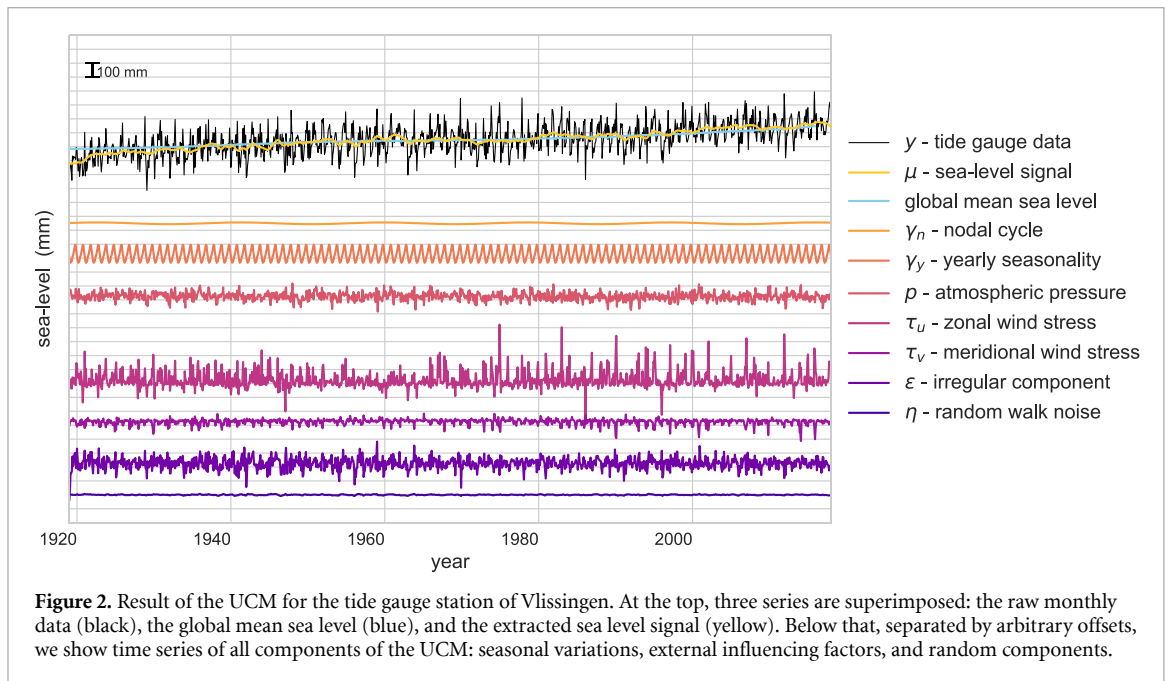
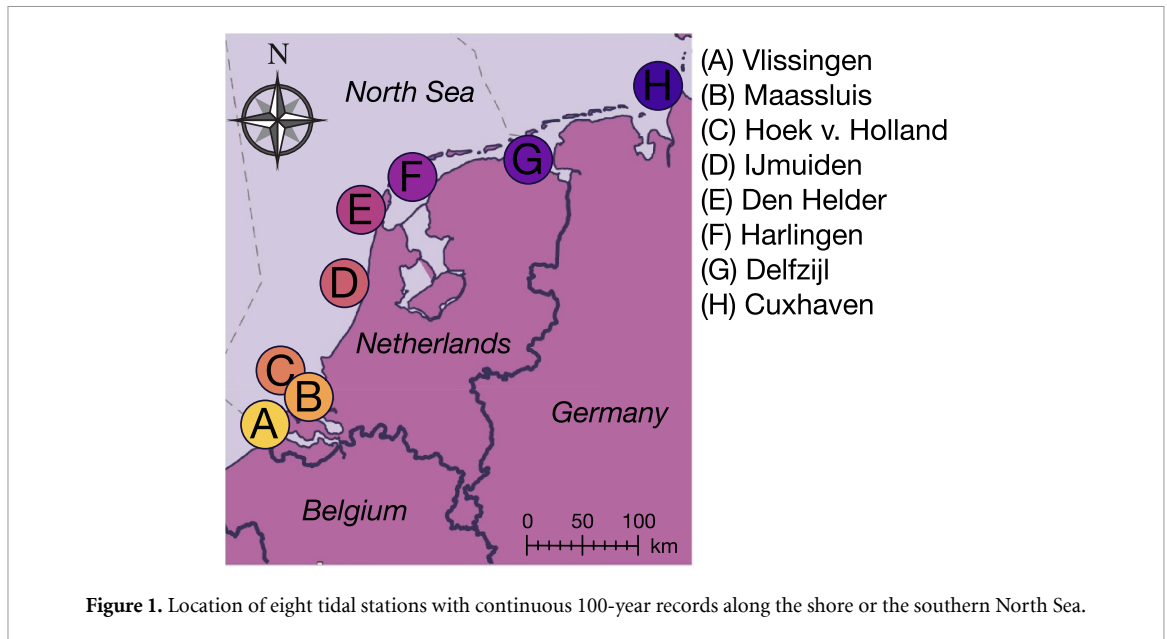
We applied the developed two-step approach to detect a breakpoint to eight tide gauges in the southern North Sea that have continuous 100-year records for the period 1919–2018 (figure 1) (Permanent Service for Mean Sea Level 2021). The air pressure and the wind in two directions are based on interpolated reanalysis products (Compo *et al* 2011, Slivinski *et al* 2019).

3. Results

3.1. Detection of SLR acceleration

Extraction of the sea-level signal from monthly averaged tide gauge data is illustrated for tidal station Vlissingen (station A in figure 1) in figure 2 and for all individual stations in the supplemental material (figure S1). The figure shows 100 years of raw monthly averaged tide gauge measurements (black line). The sea-level is clearly rising, but the measured levels vary by 30–50 cm during a year. The extracted sea-level signal (yellow) is plotted on top of the raw data. The contributions of all the described components of the UCM, which together reproduce the whole input signal, are shown by the seven colored curves plotted below the raw data. Global mean sea-level (Dangendorf *et al* 2019) is also plotted on top of the raw data (blue curve) and shows a similar trend to the extracted signal for most of the Vlissingen record.

The extracted sea-level signals for all eight stations are shown in figure 3. A PWLF consisting of two straight segments is fitted to each sea-level signal. The slope of each linear segment represents the rate of SLR. An increase in slope at the breakpoint indicates the presence of a positive acceleration in SLR. The developed Bayesian algorithm searches for a common breakpoint t^* for all stations, based on the expectation that common processes drive long-term regional SLR changes. Each station may have a different SLR (different slopes k_1 and k_2), due to the potential influence of local factors.



The fitted PWLFs are shown in figure 3 (black lines) for all stations. Our analysis detected a statistically significant increase in SLR at the common breakpoint of $t^* = 1993$. On average, SLR increased by $1.0 \pm 0.5 \text{ mm yr}^{-1}$ from $1.7 \pm 0.3 \text{ mm yr}^{-1}$ prior to 1993 to $2.7 \pm 0.4 \text{ mm yr}^{-1}$ after 1993 (black curve at bottom of figure 3). The estimated SLR varies between stations by more than 1 mm yr^{-1} , both before and after 1993 (table 1).

3.2. Robustness check

The presented results are for time series of 100 years that start in 1919. The question arises whether different results are obtained for shorter time series that start in later years or end in earlier years. To answer these questions, we first analyzed

progressively shorter time series, with a minimum length of 30 years, by increasing the starting year of the analysis from 1919 to 1988, while the end year remains fixed at 2018. The results are shown in figure 4. Detected breakpoints that are within 10 years of the beginning or end of the analyzed series are discarded, because we consider 10 years to be too short to estimate a climate-related SLR rate.

The detected breakpoints fall within a period of 7 years (1987–1994, at the 95% confidence level) when the starting year varies between 1919 and 1970 (figure 4(a)). The corresponding mean SLR rates before (\bar{k}_1) and after (\bar{k}_2) the breakpoint are fairly constant and the 95% confidence intervals of \bar{k}_1 and \bar{k}_2 are separated (figure 4(b)). This indicates that the mean SLR increase across the breakpoint is

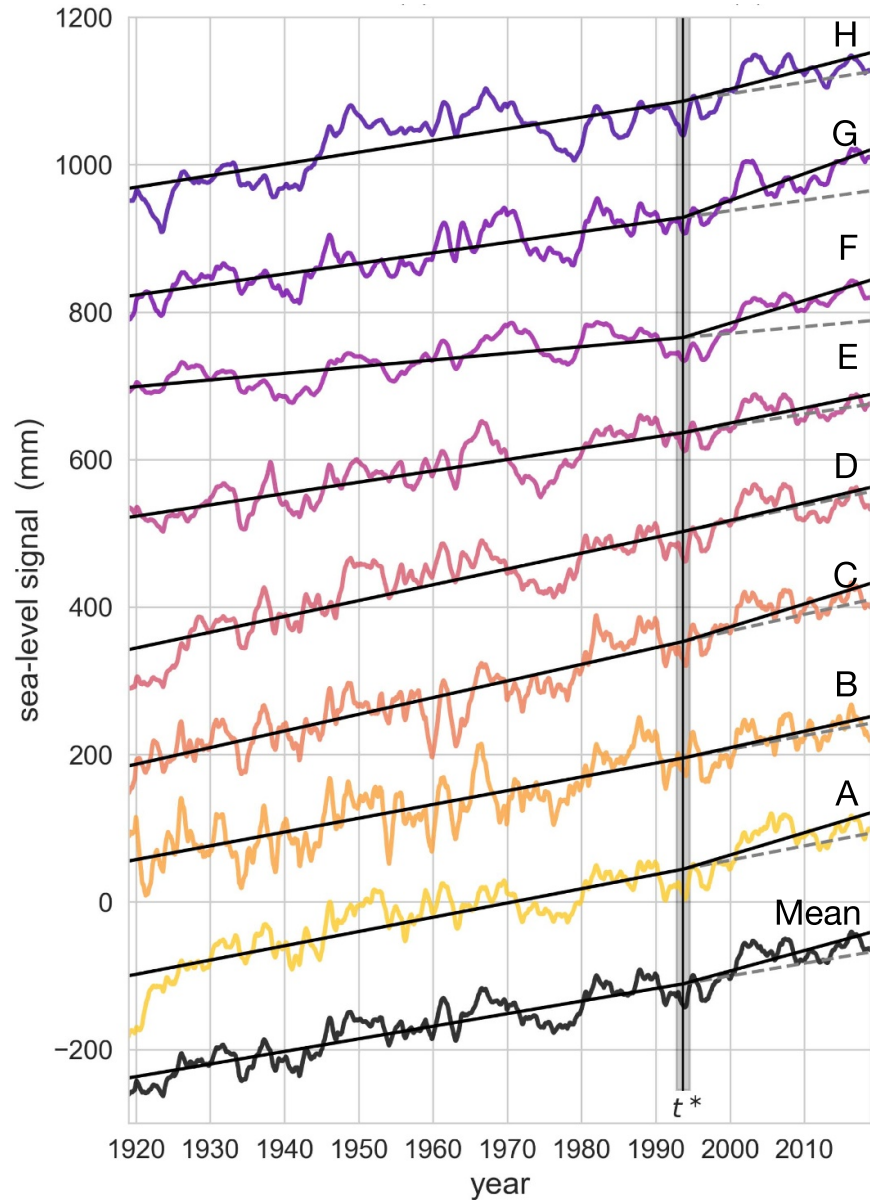
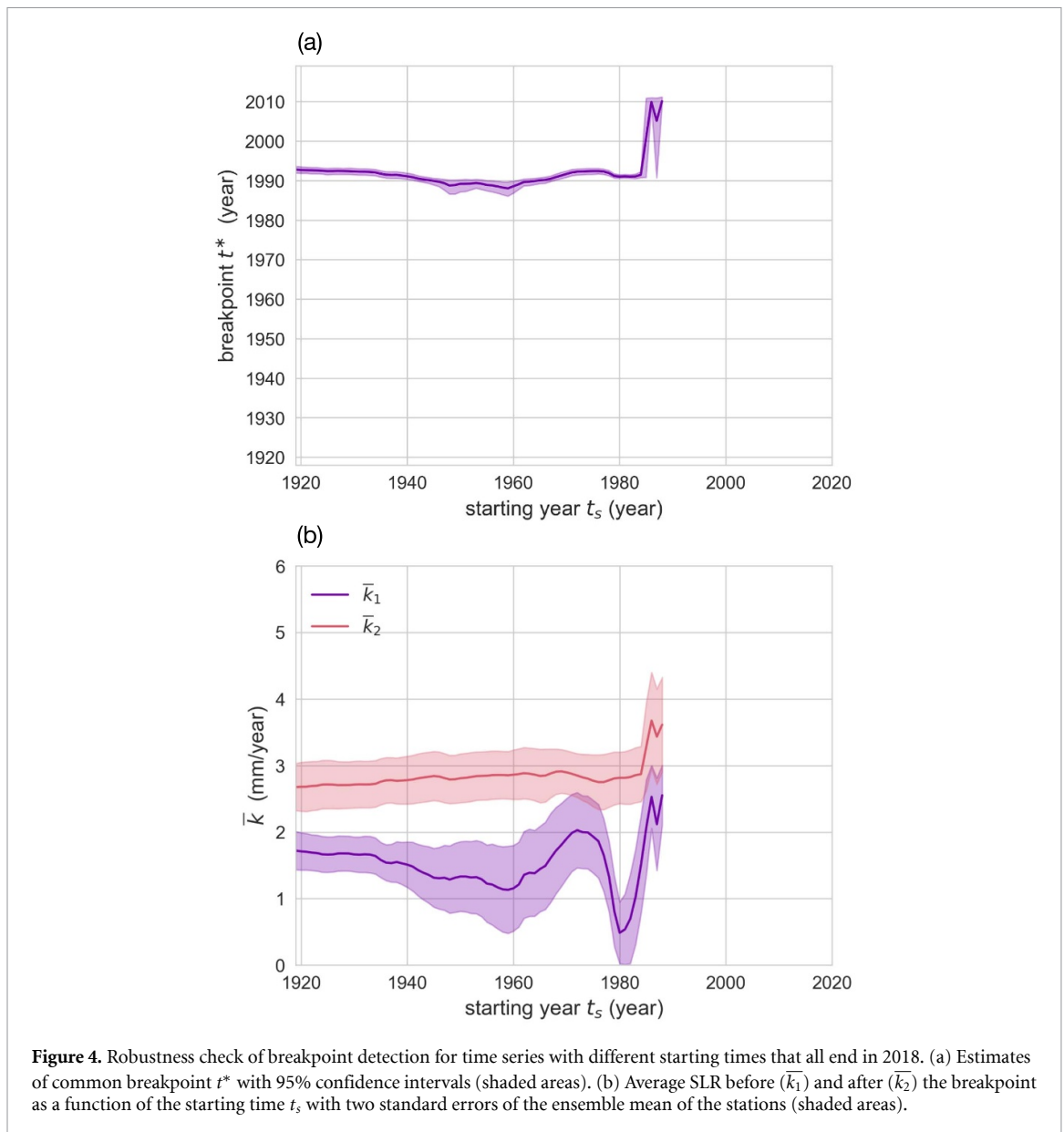


Figure 3. The extracted monthly sea-level signal (colored curves) and the fitted PWLF (black lines) from the tide gauges analyzed in this study. An arbitrary offset is added to the individual time series for better visualization. The locations of the tide gauges are shown in the inset. The detected breakpoint t^* is shown with a vertical line and the 95% confidence interval obtained with the Markov Chain Monte Carlo analysis is shaded (August 1993 \pm 11 months).

Table 1. Detailed results of the MCMC break-point detection depicted in figure 3, showing the estimated SLR of the individual stations before (k_1) and after (k_2) the common breakpoint t^* , with their corresponding 95% confidence intervals.

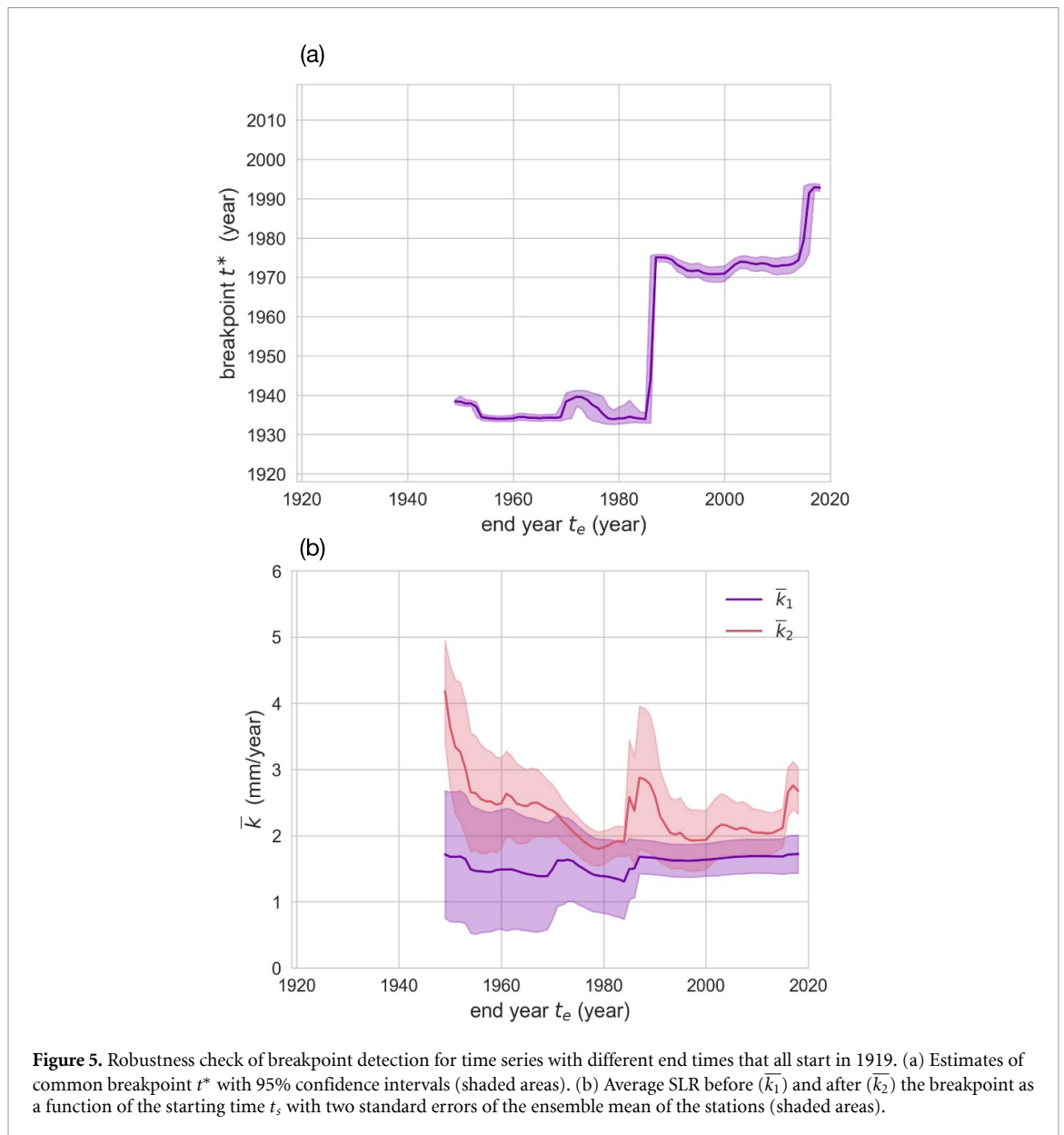
	k_1 (mm yr ⁻¹)	k_2 (mm yr ⁻¹)
(A) Vlissingen	1.96 \pm 0.06	2.9 \pm 0.2
(B) Maassluis	1.85 \pm 0.06	2.2 \pm 0.2
(C) Hoek van Holland	2.26 \pm 0.06	3.1 \pm 0.2
(D) IJmuiden	2.17 \pm 0.05	2.2 \pm 0.1
(E) Den Helder	1.55 \pm 0.06	1.9 \pm 0.2
(F) Harlingen	0.92 \pm 0.06	3.0 \pm 0.2
(G) Delfzijl	1.47 \pm 0.06	3.5 \pm 0.2
(H) Cuxhaven	1.59 \pm 0.06	2.6 \pm 0.2
Mean	1.7 \pm 0.3	2.7 \pm 0.4



statistically significant. Estimated values of k_1 and k_2 for individual stations are qualitatively similar to the average solution even though large inter-station differences are visible (figure S2, supplemental material). Results are inconsistent for time series that start after 1970 (figure 4). The estimated value of \bar{k}_1 oscillates between 0.5 and 2.5 mm yr⁻¹, and its confidence interval partly overlaps the confidence interval of \bar{k}_2 . The detected breakpoint may be unreliable for series starting around 1980, for which \bar{k}_1 is highly variable, because the detected breakpoint is close to the starting year (figure 4(b)).

Next, we reverse the previous experiment and analyze progressively shorter time series by decreasing the ending year of the analysis, from 2018 till 1948, while the starting year remains fixed at 1919. The results are shown in figures 5. Although stable breakpoints are detected in series that end in

1948–2015, none of these breakpoints are associated with a significant increase of the SLR rate, as the confidence intervals of \bar{k}_1 and \bar{k}_2 overlap. A significant increase in SLR across the breakpoint in 1993 is only detected when the series end in 2015 or later, which means that the acceleration in SLR can only be detected in the 100 year record when recent data is included. A similar result is obtained when analyzing 50 years of data starting in 1969 (figure S3, supplemental material), where it is noted that the use of this shorter record allows for an earlier detection of the breakpoint, already characterized by stable (\bar{k}_1) and (\bar{k}_2) rates for records ending around 2010. Overall, we conclude that our approach gives consistent estimates for the breakpoint and a significant increase in regional SLR rates, provided that the series start early enough and extend far enough into the 21st century.



4. Discussion and conclusions

We developed an approach to extract the ocean-driven sea-level signal from tide gauge records by taking into account two seasonal signals and three external influence factors. With respect to the influence of other low-frequency signals, due to teleconnections, we have considered the effect of the North Atlantic Oscillation (NAO) (Ezer *et al* 2016), but not included it in the final UCM for two reasons: first, the effect was very small for all stations relative to the other contributors (i.e. ten times smaller than the wind effect). Second, the regression coefficients were not statistically significant for most of the stations (table S2, supplemental material). As an example, the extracted signals at Cuxhaven with and without adding the NAO as a regressor in the UCM are shown in the supplemental material (figure S4).

We detected a common breakpoint in the extracted sea-level signals from a regional set of tide gauge stations. The estimation of a common breakpoint is crucial to the success of the detection, because it results in a reduced sensitivity to inter-station differences, as shown by the fact that a significant trend change across the common breakpoint is not always present at all stations for all starting years (figure S2). An ensemble detection is justified because regional SLR acceleration is a large-scale phenomenon that is most likely caused by a common and remote driver, which for the North Sea will be a combination of stereodynamic changes originating in the deeper North Atlantic (Landerer *et al* 2007) and of worldwide continental freshwater fluxes (Bamber and Riva 2010). The magnitude of SLR before and after the breakpoint was independently estimated for each station and averaged afterwards.

We detected, for the first time, a breakpoint in regional SLR in the tide gauge records along the southern North Sea. The mean SLR increased by $1.0 \pm 0.5 \text{ mm yr}^{-1}$ after 1993, reaching a value of $2.7 \pm 0.4 \text{ mm yr}^{-1}$. The detected breakpoint reveals a long-term increase in SLR that is unprecedented in the regional instrumental record. These findings are robust with respect to the length of the record, provided that observations start before the 1970s and end in 2015 or later.

The estimated average SLR after the breakpoint is in agreement with results by Frederikse *et al* (2020) for the larger Subpolar North Atlantic basin, where their tide gauge reconstruction provides a value of $2.7 \pm 0.6 \text{ mm yr}^{-1}$ for the same period (without GIA correction and with uncertainty scaled to 95% confidence). The SLR trend is also in line with the global mean value of $3.1 \pm 0.4 \text{ mm yr}^{-1}$ since 1993 (Dangendorf *et al* 2017, 2019, Cazenave *et al* 2018, Frederikse *et al* 2020). However, its physical interpretation may differ, due to regional variability in vertical land motion and gravity changes induced by the glacial isostatic adjustment signal of the last ice age (Walcott 1972, Farrell and Clark 1976, Peltier and Andrews 1976), as well as to local variability in vertical land motion of different origin including tectonics. We ignore the effect of local processes, such as groundwater extraction, because we do not expect them to have a significant impact on either the determination of the common breakpoint, by design of the detection algorithm, or on the trend change across the breakpoint, which can only be contaminated by a local process with a time evolution similar to that of the sea level signal. The subsidence signal induced by tectonics in the region is expected to be smaller than 0.2 mm yr^{-1} (Kiden *et al* 2002), which is less than our trend uncertainty and can therefore be neglected. Concerning the effect of glacial isostatic adjustment, according to recent work (Simon *et al* 2021), its contribution to our estimates of regional mean SLR amounts to $0.9 \pm 0.7 \text{ mm yr}^{-1}$ (95% confidence), and is not expected to change for several centuries. The net contribution of ocean-driven SLR rates may be obtained by removing the contribution of glacial isostatic adjustment, which gives net SLR rates before and after the breakpoint of $\bar{k}_1 = 0.8 \pm 0.8 \text{ mm yr}^{-1}$ and $\bar{k}_2 = 1.9 \pm 0.8 \text{ mm yr}^{-1}$, respectively. This means that the SLR rate before and after the detected breakpoint has potentially more than doubled.

Along the North Sea, both the UK and the Netherlands have adopted future-oriented flood risk management strategies that critically depend on the monitoring of SLR (Bloemen *et al* 2018, 2019). The detected acceleration in regional SLR constitutes salient information for countries in the southern North Sea to plan adaptive action and provide engineers with the basic data required for their designs. Our method may be applied to any coastal region with

sufficiently long tidal records that are in need of salient information to plan for adaptation to SLR. Our analysis indicates that SLR records of at least 40 years should be sufficient for this purpose. Current SLR scenarios (Masson-Delmotte *et al* 2021) still grant vulnerable coastal communities time to accumulate the required time series to support planning for future-oriented flood risk management in the second half of this century.

Author contributions

D B S and R E M R designed the study with input from all authors. D B S performed the computations and produced the figures. D B S, R E M R and M B drafted the manuscript. All authors commented on the results and edited the manuscript.

Data availability statement

The data that support the findings of this study are openly available. Tide gauge data can be downloaded from PSMSL at: www.psmsl.org/data/.

Air pressure and wind speed reanalysis products can be downloaded from NOAA at: www.esrl.noaa.gov/psd/data/gridded/data.ncep.reanalysis.derived.surface.html

The source code and output of the UCM analysis, as shown in figure 2, figure 3 and figure S1, is available at https://github.com/steffelbauer/sea_level_rise_acceleration

Acknowledgment

This research was sponsored by the Climate Institute of Delft University of Technology.

ORCID iDs

David B Steffebauer  <https://orcid.org/0000-0003-2137-985X>

Riccardo E M Riva  <https://orcid.org/0000-0002-2042-5669>

Jos S Timmermans  <https://orcid.org/0000-0002-2759-7893>

Mark Bakker  <https://orcid.org/0000-0002-5629-2861>

References

- Bamber J and Riva R 2010 The sea level fingerprint of recent ice mass fluxes *Cryosphere* **4** 621–7
- Bloemen P, Reeder T, Zevenbergen C, Rijke J and Kingsborough A 2018 Lessons learned from applying adaptation pathways in flood risk management and challenges for the further development of this approach *Mitigation Adaptation Strateg. Glob. Change* **23** 1–26
- Bloemen P, van der Steen M and van der Wal Z 2019 Designing a century ahead: climate change adaptation in the Dutch Delta *Policy Soc.* **38** 58–76

- Calafat F and Chambers D 2013 Quantifying recent acceleration in sea level unrelated to internal climate variability *Geophys. Res. Lett.* **40** 3661–6
- Cash D, Clark W, Alcock F, Dickson N, Eckley N, Guston D, Jaeger J and Mitchell R 2003 Knowledge systems for sustainable development *Proc. Natl Acad. Sci.* **100** 8086–91
- Cazenave A, Meyssignac B, Ablain M, Balmaseda M, Bamber J, Barletta V, Beckley B, Benveniste J, Berthier E and Blazquez A 2018 Global sea-level budget 1993–present *Earth Syst. Sci. Data* **10** 1551–90
- Compo G P *et al* 2011 The twentieth century reanalysis project *Q. J. R. Meteorol. Soc.* **137** 1–28
- Dangendorf S, Calafat F M, Arns A, Wahl T, Haigh I D and Jensen J 2014 Mean sea level variability in the North Sea: processes and implications *J. Geophys. Res.: Oceans* **119** 6820–41
- Dangendorf S, Hay C, Calafat F M, Marcos M, Piecuch C G, Berk K and Jensen J 2019 Persistent acceleration in global sea-level rise since the 1960s *Nat. Clim. Change* **9** 705–10
- Dangendorf S, Marcos M, Wöppelmann G, Conrad C P, Frederikse T and Riva R 2017 Reassessment of 20th century global mean sea level rise *Proc. Natl Acad. Sci.* **114** 5946–51
- Davis J L and Vinogradova N T 2017 Causes of accelerating sea level on the east coast of North America *Geophys. Res. Lett.* **44** 5133–41
- Durbin J and Koopman S J 2013 *Time Series Analysis by State Space Methods* (Oxford: Oxford University Press)
- Ezer T, Haigh I D and Woodworth P L 2016 Nonlinear sea-level trends and long-term variability on western European coasts *J. Coast. Res.* **32** 744–55
- Farrell W and Clark J A 1976 On postglacial sea level *Geophys. J. Int.* **46** 647–67
- Frederikse T *et al* 2020 The causes of sea-level rise since 1900 *Nature* **584** 393–7
- Frederikse T and Gerkema T 2018 Multi-decadal variability in seasonal mean sea level along the north sea coast *Ocean Sci.* **14** 1491–501
- Frederikse T, Riva R, Kleinherenbrink M, Wada Y, van den Broeke M and Marzeion B 2016 Closing the sea level budget on a regional scale: trends and variability on the northwestern European continental shelf *Geophys. Res. Lett.* **43** 10–864
- Haasnoot M, Kwadijk J, Van Alphen J, Le Bars D, Van Den Hurk B, Diermanse F, Van Der Spek A, Oude Essink G, Delsman J and Mens M 2020 Adaptation to uncertain sea-level rise; how uncertainty in Antarctic mass-loss impacts the coastal adaptation strategy of the Netherlands *Environ. Res. Lett.* **15** 034007
- Haasnoot M, Lawrence J and Magnan A 2021 Pathways to coastal retreat *Science* **372** 1287–90
- Haasnoot M, van 't Klooster S and van Alphen J 2018 Designing a monitoring system to detect signals to adapt to uncertain climate change *Glob. Environ. Change* **52** 273–85
- Haigh I D, Wahl T, Rohling E J, Price R M, Pattiaratchi C B, Calafat F M and Dangendorf S 2014 Timescales for detecting a significant acceleration in sea level rise *Nat. Commun.* **5** 3635
- Harvey A C 1990 *Forecasting, Structural Time Series Models and the Kalman Filter* (Cambridge: Cambridge University Press)
- Hoffman M D and Gelman A 2014 The No-U-turn sampler: adaptively setting path lengths in Hamiltonian Monte Carlo *J. Mach. Learn. Res.* **15** 1593–623 (available at: www.jmlr.org/papers/volume15/hoffman14a/hoffman14a.pdf)
- James G, Witten D, Hastie T and Tibshirani R 2013 *An Introduction to Statistical Learning* vol 112 (Berlin: Springer)
- Kaye C A and Stuckey G W 1973 Nodal tidal cycle of 18.6 yr.: its importance in sea-level curves of the east coast of the United States and its value in explaining long-term sea-level changes *Geology* **1** 141–4
- Kiden P, Denys L and Johnston P 2002 Late quaternary sea-level change and isostatic and tectonic land movements along the Belgian–Dutch North Sea coast: geological data and model results *J. Quat. Sci.* **17** 535–46
- Landerer F W, Jungclaus J H and Marotzke J 2007 Ocean bottom pressure changes lead to a decreasing length-of-day in a warming climate *Geophys. Res. Lett.* **34** L06307
- Mach K J and Siders A 2021 Reframing strategic, managed retreat for transformative climate adaptation *Science* **372** 1294–9
- Masson-Delmotte V *et al* (eds) 2021 IPCC, 2021: summary for policymakers *Climate Change 2021: The Physical Science Basis. Contribution of Working Group I to the Sixth Assessment Report of the Intergovernmental Panel on Climate Change* (Cambridge University Press)
- Moss R, Reed P M, Hadjimichael A and Rozenberg J 2021 Planned relocation: pluralistic and integrated science and governance *Science* **372** 1276–9
- Mudelsee M 2019 Trend analysis of climate time series: a review of methods *Earth-Sci. Rev.* **190** 310–22
- Peltier W R and Andrews J T 1976 Glacial-isostatic adjustment—I. The forward problem *Geophys. J. Int.* **46** 605–46
- Permanent Service for Mean Sea Level 2021 Obtaining tide gauge data (available at: www.psmsl.org/data/obtaining/) (Accessed 21 March)
- Raso L, Kwakkel J H and Timmermans J 2019a Assessing the capacity of adaptive policy pathways to adapt on time by mapping trigger values to their outcomes *Sustainability* **11** 1716
- Raso L, Kwakkel J, Timmermans J and Panthou G 2019b How to evaluate a monitoring system for adaptive policies: criteria for signposts selection and their model-based evaluation *Clim. Change* **153** 267–83
- Richter K *et al* 2020 Detecting a forced signal in satellite-era sea-level change *Environ. Res. Lett.* **15** 094079
- Salvatier J, Wiecki T V and Fonnesbeck C 2016 Probabilistic programming in Python using PyMC3 *PeerJ Comput. Sci.* **2** e55
- Seabold S and Perktold J 2010 Statsmodels: econometric and statistical modeling with python *9th Python in Science Conf.* (<https://doi.org/10.25080/Majora-92bf1922-011>)
- Simon K, Riva R and Vermeersen L 2021 Constraint of glacial isostatic adjustment in the North Sea with geological relative sea level and GNSS vertical land motion data *Geophys. J. Int.* **227** 1168–80
- Slivinski L C *et al* 2019 Towards a more reliable historical reanalysis: improvements for version 3 of the twentieth century reanalysis system *Q. J. R. Meteorol. Soc.* **145** 2876–908
- Vinogradov S V and Ponte R M 2011 Low-frequency variability in coastal sea level from tide gauges and altimetry *J. Geophys. Res.: Oceans* **116** C07006
- Wahl T, Haigh I D, Woodworth P L, Albrecht F, Dillingham D, Jensen J, Nicholls R J, Weisse R and Wöppelmann G 2013 Observed mean sea level changes around the north sea coastline from 1800 to present *Earth Sci. Rev.* **124** 51–67
- Walcott R 1972 Past sea levels, eustasy and deformation of the earth *Quat. Res.* **2** 1–14
- Woodworth P L 2012 A note on the nodal tide in sea level records *J. Coast. Res.* **28** 316–23